Dynamic behavior of earth dams under short-term semi-harmonic loads

Karim Sultanov[1] and *Sadillakhon* Umarkhonov[1*]

[1]Institute of Mechanics and Seismic Stability of Structures, Tashkent, Uzbekistan

Abstract. The article is devoted to the dynamic problems of studying the strain state of earth dams under dynamic impacts. A method is developed for solving wave problems to determine the stress-strain state of earth structures, in particular, earth dams. Based on the use of the finite difference method, an algorithm for solving problems and calculation formulas were developed that have second-order accuracy in time and coordinates. The advantage of the developed method is the implementation of complex nonlinear deformation models, taking into account structural changes and moisture content of soil. In the example of the Charvak dam, the distribution of the stress state over the cross-section of the dam under the action of its own weight is determined and the problem of the dynamic behavior of an earth dam under the influence of short-term harmonic loads is numerically solved. The change in intense stresses at some points of the earth dam over time is determined.

1 Introduction

It is known that damage to earth dams causes great losses, therefore, in design and construction, it is necessary to perform calculations for their strength and reliability. However, the processes that determine the pattern of operation of an earth dam have not yet been studied sufficiently, considering the nonlinear deformations of the dam material. The prediction of changes in stresses and strains occurring in earth dams under the influence of various loads (dead weight of soil, seismic impact) is based on the description of the patterns of soil strain and its strength under stress conditions [1, 2]. A significant impact on the stress and strain distribution in soils exerts physical and mechanical characteristics in the body and foundation of the dam, geometric parameters of the structure, fluctuations in the level of the reservoir filling, seismic impacts, etc. Numerical methods are often used to determine the stress-strain state of dams [3-6]. At the same time, the values of stress and strain indices should be determined based on the analysis of a number of parameters, including the results of calculations of the stress-strain state of an earth dam. Many scientists conduct research work on the strength of earth dams using numerical methods [8-22].

* Corresponding author: umarkhonov@gmail.com

2 Statement and solution to the problem

Consider earth dams on a rigid foundation (Fig. 1). If the length of the dam is very large compared to its width and height, its motion can be considered plane-deformed. Under the influence of dynamic forces on the foundations of earth dams (Fig. 2), the particles of the dam medium begin to move. The equation of motion of an earth dam has the following form [1, 2]:

$$\rho\frac{d\upsilon_x}{dt}=\frac{\partial S_{xx}}{\partial x}+\frac{\partial P}{\partial x}+\frac{\partial \tau_{xy}}{\partial y},\quad \rho\frac{d\upsilon_y}{dt}=\frac{\partial S_{yy}}{\partial y}+\frac{\partial P}{\partial y}+\frac{\partial \tau_{xy}}{\partial x}-\rho g \tag{1}$$

where υ_x, υ_y are the particle velocities in x and y directions; S_{xx}, S_{yy}, τ_{xy} are the deviator stress components; ρ is the density of the medium; P is the pressure.
Naturally, the total stresses are determined by the following formulas:

$$\sigma_{xx}=S_{xx}+\mathrm{P},\quad \sigma_{yy}=S_{yy}+\mathrm{P},\quad \sigma_{zz}=S_{zz}+\mathrm{P}. \tag{2}$$

The dam deformation model is taken in the form of nonlinear equations [3, 4]:

$$\dot{P}=-\left(\lambda+\frac{2}{3}\mu\right)\frac{\dot{V}}{V}, \tag{3}$$

$$\frac{dS_{xx}}{dt}+\lambda S_{xx}=2G\left(\frac{d\varepsilon_{xx}}{dt}-\frac{dV}{3Vdt}\right),\quad \frac{dS_{yy}}{dt}+\lambda S_{yy}=2G\left(\frac{d\varepsilon_{yy}}{dt}-\frac{dV}{3Vdt}\right), \tag{4}$$

$$\frac{dS_{zz}}{dt}+\lambda S_{zz}=2G\left(\frac{d\varepsilon_{zz}}{dt}-\frac{dV}{3Vdt}\right),$$

$$\frac{d\tau_{xy}}{dt}+\lambda\tau_{xy}=2G\frac{d\tau_{xy}}{dt}.$$

The general dependence of the ultimate strength on the pressure in the generalized von Mises condition has the following form

$$S_{xx}^2+S_{yy}^2+S_{zz}^2+2\tau_{xy}^2\le\frac{2}{3}\left[Y(P)\right]^2 \tag{5}$$

$$Y(P)=Y_0+\frac{\mu P}{1+\mu P/(Y_{PL}-Y_0)} \tag{6}$$

here K and G are the moduli of volumetric compressions and shear, respectively; $V=\rho_0/\rho$ is the relative volume; Y_0 is the cohesion; μ is the coefficient of friction; Y_{PL} is the limiting value of resistance to rock backfill shear, λ is the functional defined by the following formulas:

$$\lambda=\frac{3W}{2Y^2}H(W),\quad H(W)=\begin{cases}1, & \text{at } W\ge 0\\ 0, & \text{at } W<0\end{cases},$$

$$W = 2\mu\left\{\sum_{j=x,y,z} S_{jj}\left(\frac{d\varepsilon_{jj}}{dt} - \frac{1}{3}\frac{dV}{Vdt}\right) + \tau_{xy}\frac{d\varepsilon_{xy}}{dt}\right\}. \quad (7)$$

It is necessary to add relations that connect the components of strain rates with mass velocities, and the soil continuity equation [5] to the system of equations (1)–(7):

$$\frac{d\varepsilon_{xx}}{dt} = \frac{\partial U_x}{\partial x} \qquad \frac{d\varepsilon_{yy}}{dt} = \frac{\partial U_y}{\partial y} \qquad \frac{d\varepsilon_{xy}}{dt} = \frac{1}{2}\left(\frac{\partial U_y}{\partial x} + \frac{\partial U_x}{\partial y}\right). \quad (8)$$

$$\frac{dV}{dt} - V\cdot\left(\frac{\partial U_x}{\partial x} + \frac{\partial U_y}{\partial y}\right) = 0 \quad . \quad (9)$$

Thus, the system of differential equations (1)–(9) is closed, and using initial and boundary conditions, it describes the complete pattern of the dynamic behavior and stress-strain state of an earth dam. On the slopes and the crest of the dam, the conditions are considered stress-free. The initial conditions are taken equal to zero.

The geometric dimensions of the earth dam are height - 168 m, top width – 12 m, bottom width – 664 m, the slope of the upstream face - 1:2, the slope of the downstream face - 1:1.9, the width of the central core - 110 and 12 m. The physical and mechanical parameters of an earth dam are [1, 6]: for a slope, the density is 1980 kg/m^3, elasticity modulus - E_{dam} = 6210 MPa, Poisson's ratio - ν_{dam} = 0.3; slope strength indicators are (cohesion, coefficient of friction, ultimate shear strength) – Y_0=μ/800, μ=0.4, Y_{dam}=20·Y_0. For a core, the density is 1760 kg/m^3; modulus of elasticity – E_{core}=3105 MPa; Poisson's ratio – ν_{core}==0.3; slope strength indicators are (cohesion, friction coefficient, ultimate shear strength) – Y_0=μ/1000, μ=0.3, Y_{core}=20·Y_0.

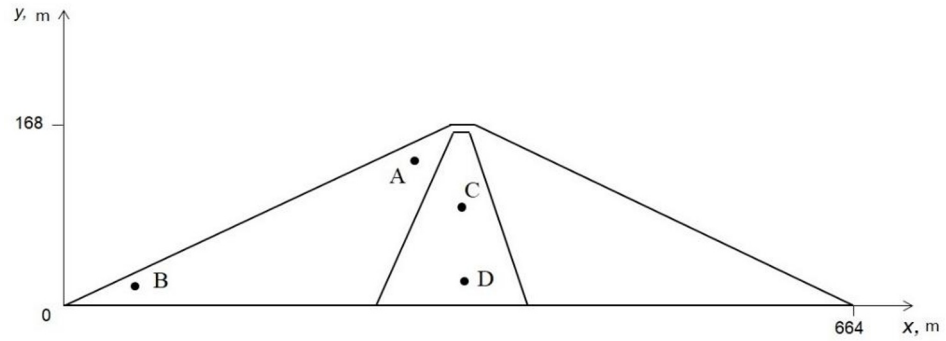

Fig. 1. Cross-section of an earth dam.

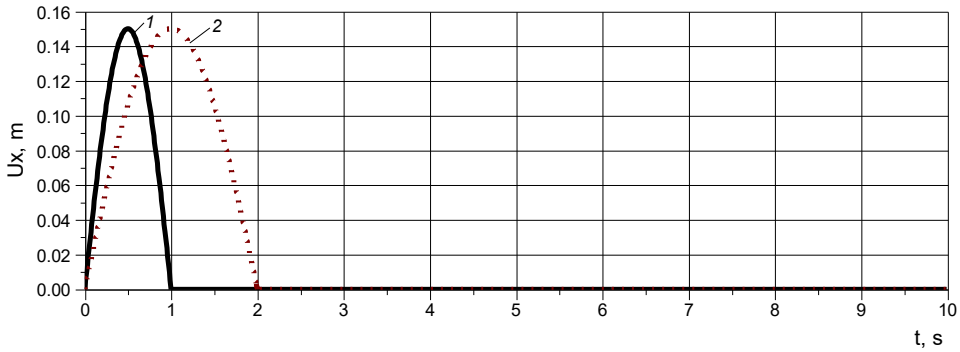

Fig. 2. Dynamic impact.

3 Solution method

Let us consider the numerical solutions to the problems posed by the difference method using the scheme proposed by M. Wilkins [7] for a quadrangular cell. In non-stationary problems, one independent variable, the time t variable, is of particular importance. Discretization of the problem with respect to this variable means that the calculation is performed with discrete time steps, each of which represents the transition from the state at t0 to the state at t0+Δt. The advantage of the Wilkins scheme [7] is that in the calculations the time step Δt is realized by an automatic choice from the stability and accuracy conditions, and it can change every time [7].

4 Numerical results

Harmonic forces shown in Fig.1 are taken as dynamic forces. Under the action of a harmonic load on the foundation of an earth dam, particles in the body of the dam begin to move, i.e. inside the dam, the soil is deformed. Harmonic load is taken for four options, i.e. for different frequencies of the half-sine wave, as shown in Fig. 2: 1 - t=1.0 s, 2 - t=2.0 s. Boundary and initial conditions: it is assumed that the dam is not strained and is at rest before dynamic loading. The slopes and the crest are stress-free.

The results of solving this problem are presented graphically. Figure 3 shows the change in σx , σy in the near-crest zone of the dam (at point A) under harmonic loading. In these figures, the 1st curve denotes the stress at point A under dynamic half-sinusoidal load, which has a period of 1.0 s. The 2nd curve denotes the stress at point A under dynamic half-sinusoidal load, which has a period of 2.0 s. Maximum values of horizontal stresses 0.75-0.85 MPa appear at t=2-4 s, and then they decrease to 0.5 MPa at t=10 s, see Fig. 3. Maximum values of vertical stresses at point A appear at t=6-8 s, and then they stabilize at t=10 s and take values of 0.12-0.15 MPa.

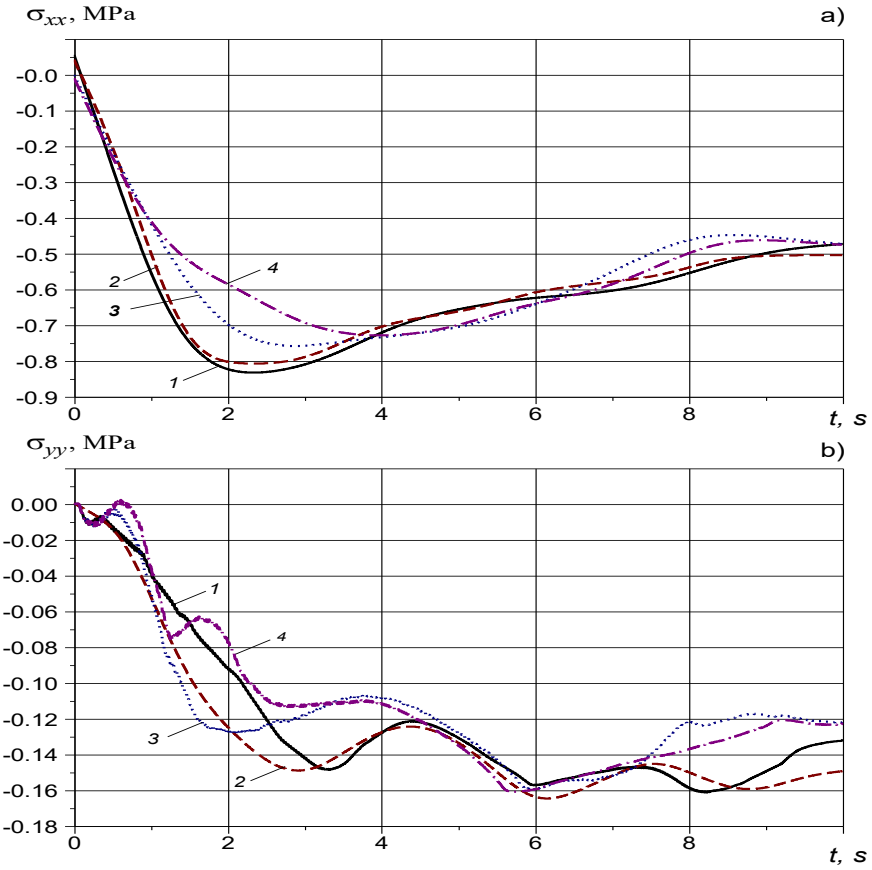

Fig. 3. Change in stresses at point A over time

Figure 4 shows the change in horizontal and vertical stresses at point B. In these figures, the 1st curve corresponds to the stress at point B under dynamic half-sinusoidal load with a period of 0.25 s. The 2nd curve denotes the stress at point B under dynamic half-sinusoidal load, which has a period of 0.5 s. The 3rd curve denotes the stress at point B under dynamic half-sinusoidal load with a period of 1.0 s.

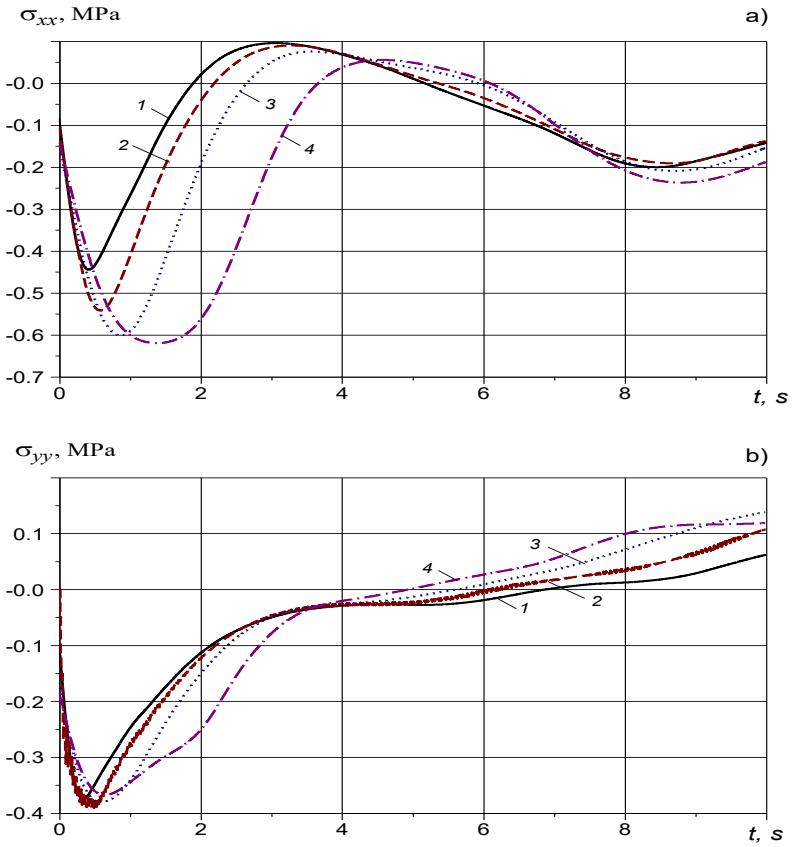

Fig. 4. Change in stresses at point B over time.

The 4th curved line denotes the stress at point B under dynamic half-sinusoidal load, with a period of 2.0 s, (Fig. 4). Maximum values of horizontal stresses 0.5-0.6 MPa, appear at t=0.3-2 s and then they decrease to 0.15-0.19 MPa at t=10 s (Fig. 4, a). Maximum values of vertical stresses at point B appear at t=0.2-0.6 s, and then they stabilize at t=10 s and take values of 0.05-0.14 MPa (Fig. 4,b).

The change in horizontal and vertical stresses in the center of the dam (at point C) is shown in Fig. 5. Here, too, the 1st curved line denotes the stress at point C under dynamic half-sinusoidal load with a period of 1.0 s. The 2nd curved line denotes the stress at point C under dynamic half-sinusoidal load with a period of 2.0 s. Maximum values of horizontal stresses appear at t=0.8-2.5 s and they are 0.23–-0.27 MPa, and then the amplitude decreases, and at time point t=10 s, they take the values of 0.11- 0.20 MPa (Fig. 5a). Maximum values of vertical stresses at point C appear at t=0.3-0.8 s, then they stabilize, and at the time point t=10 s they reach a value of 0.21-0.25 MPa (Fig. 5,b).

The change in horizontal and vertical stresses at the base of the center of the dam (at point D) is shown in Fig. 6. In these figures, the 1st curved line denotes the stress at point D under dynamic half-sinusoidal load with a period of 1.0 s. The 2nd curved line denotes the stress at point D with dynamic half-sinusoidal load, with a period of 2.0 s (Fig. 6). Maximum values of horizontal stresses appear after the time point t=6.0 s and they have a value of -0.52 MPa, and then they stabilize at t=10 s (Fig. 6,a). Maximum values of vertical stresses at point D appear after the time point t=6.0 s, and then they stabilize at t=10 s (Fig. 6,b).

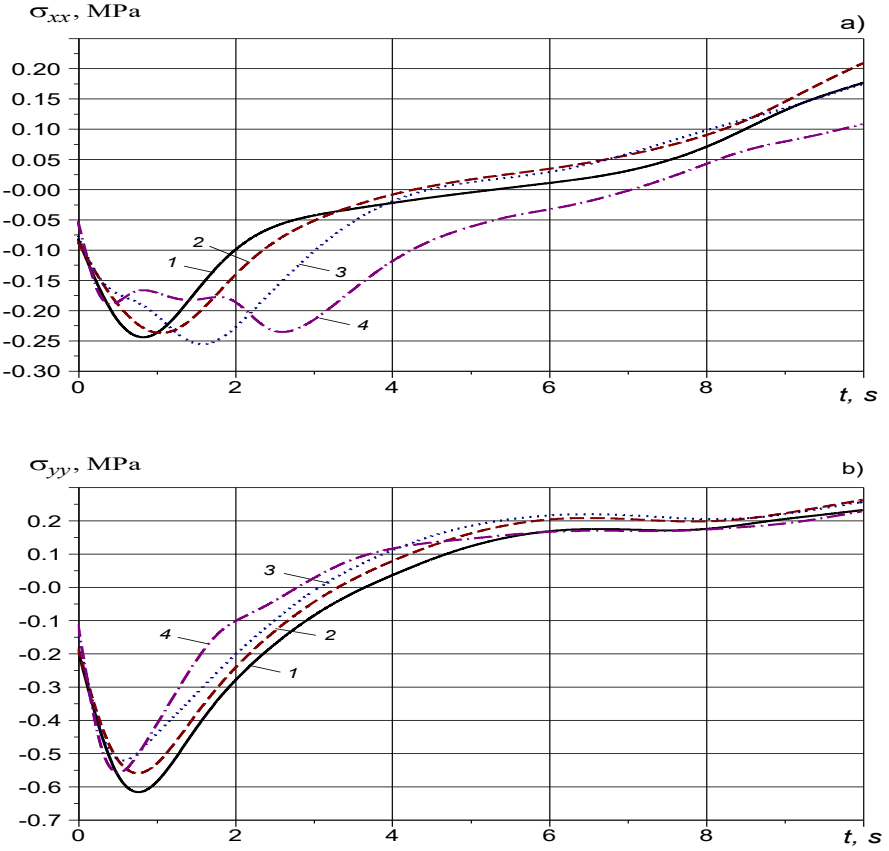

Fig. 5. Change in stresses at point C over time

Figure 7 shows the change in stress intensity at characteristic points of the dam under harmonic loading. In these figures, the 1st curved line indicates the stress intensity at point A under dynamic half-sinusoidal load. The 2nd curve indicates the stress intensity at point B under dynamic half-sinusoidal load. The 3rd curve denotes the stress intensity at point C under dynamic half-sinusoidal load. The 4th curve denotes the stress intensity at point D under dynamic half-sinusoidal load. Maximum stress intensity values 2.7 MPa appear after 1 second at point D and then the values do not change until 10 seconds, see Fig. 7, a. Maximum stress intensity values 3.4 MPa appear after 1.8 seconds at point D and then the values do not change until 10 seconds, Fig. 7,b.

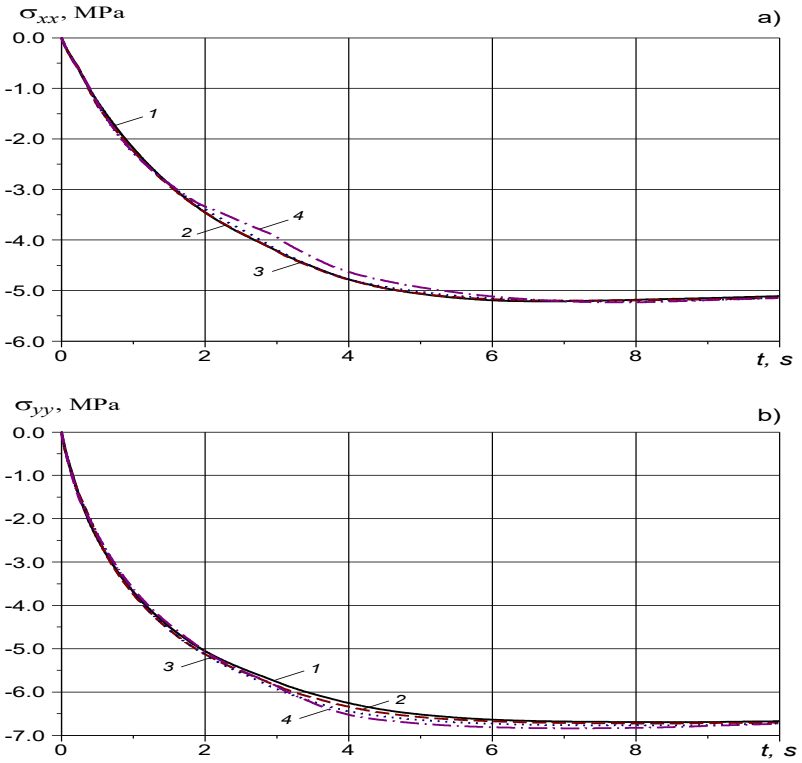

Fig.6. Change in stresses at point D over time

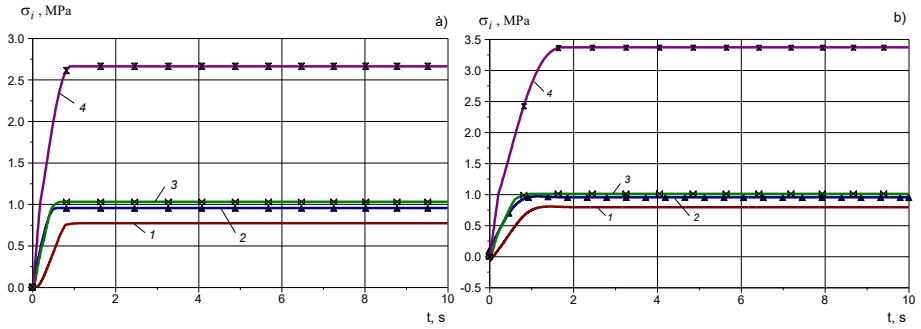

a) under the load of a period of 1 s. b) under the load of a period of 2 s.

Fig. 7. Change in stress intensity at characteristic points of the dam over time.

5 Conclusion

The main correlations of the problem of determining the stress-strain state of earth dams under dynamic influences in a plane statement are given. On the basis of the finite difference method, a solution technique is given with regard to the posed two-dimensional problem of the dynamics of deformable rigid bodies for quadrangular cells. Numerical solutions are obtained for the stress-strain state of an earth dam in the example of the Charvak dam under the impact of a harmonic load from the foundation.

References

1. K. Sultanov, S. Umarkhonov, S. Normatov. AIP Conference Proceedings **2637**, (2022) https://doi.org/10.1063/5.0118430,
2. S.I. Umarkhonov, Europaische Fachhochschule, J. V **9,** 5 (2015)
3. K.S. Sultanov, B.E. Khusanov, Foundations, foundations and soil mechanics. J. **3**, 5 (2001)
4. K.S. Sultanov, B.E. Khusanov, Foundations, bases, and soil mechanics. J. **3**, 3 (2002)
5. B.E. Khusanov, B.B. Rikhsieva, E3S Web Conf. **97**, 04040 (2019) https://doi.org/10.1051/ e3sconf/20199704040,
6. B. Khusanov, O. Khaydarova, E3S Web Conf. **97**, 05043 (2019) https://doi.org/10.1051/e3sconf/20199705043,
7. M.L. Wilkins, Computer Simulation of Dynamic Phenomena (Springer, Berlin, 2010)
8. R.A. Abirov, B.E. Khusanov, D.A. Sagdullaeva, IOP Conf. Series Material Science. Engineering **971**, 032017 (2020) https://doi.org/10.1088/1757899X/971/3/032 017,
9. Z. Ma, F. Dang, H. Liao, Y. Cheng, Arabian Journal of Geosciences. J. **13(17)**, 827 (2020) https://doi.org/10.1007/s12517-020-05851-4
10. Z. Kahot, R. Dkiouak, A. Khamlichi, International Review of Applied Sciences and Engineering **10(1)**, (2019) https://doi.org/10.1556/1848.2018.0011
11. A.T. Siacara, G.F. Napa-García, A.T. Beck, M.M. Futai, J. of Rock Mech. and Geot. Eng., J. **V12(2)**, (2020) https://doi.org/10.1016/j.jrmge.2019.07.012
12. S. Liu, L. Wang, Z. Wang, E. Bauer, J. **V9(3)**, 8 (2016) https://doi.org/https://doi.org/10.1016/j.wse.2016.11.002
13. M.M. Zanjani, A. Soroush, M. Khoshini, Soil Dynamics and Earthquake Engineering **V88**, 12 (2016) https://doi.org/https://doi.org/10.1016/j.soildyn.2016.05.012
14. X. Yang, S. Chi, Soil Dynamics and Earthquake Engineering, J. **V64**, 10 (2014) https://doi.org/https://doi.org/10.1016/j.soildyn.2014.04.007,
15. C. Liu, L. Zhang, B. Bai, J. Chen, J. Wang, Procedia Engineering, J. **V31**, 5 (2012) https://doi.org/https://doi.org/10.1016/j.proeng.2012.01.1058
16. H. Alateya, A. Ahangar Asr, Engineering Computations (Swansea, Wales) **V37(4)**, (2020) https://doi.org/10.1108/EC-03-2019-0101
17. B. Ebrahimian, Frontiers of Architecture and Civil Engineering in China J. **V5(1)**, 17 (2011) https://doi.org/10.1007/s11709-010-0082-6
18. N.J. Al-Mansori, T.A.Al-Fatlawi, N.Y. Othman, L.S. Al-Zubaidi, Civil Engineering Journal, J. **V6(7)**, 13 (2020) https://doi.org/10.28991/cej-2020-03091552,
19. S. Nimbalkar, V.S. Annapareddy, A. Pain, Journal of Rock Mechanics and Geotechnical Engineering **10(6)**, 9 (2018) https://doi.org/https://doi.org/10.1016/j.jrmge.2018.06.003
20. W. Jing, J. Wang, Journal of Vibroengineering, J **V22(2)**, 13 (2020) https://doi.org/10.21595/jve.2019.20754
21. H. Alateya, A. Ahangar, Engineering Computations (Swansea, Wales), J **V37(4)**, (2020) https://doi.org/10.1108/EC-03-2019-0101
22. M. Mirsaidov, T. Sultanov, J. Yarashov, Z, Urazmukhammedova. IOP Conference Series: Materials Science and Engineering **883(1)**, (2020) https://doi.org/10.1088/1757-899X/883/1/012021